Advances in Condensed Matter Physics

RESEARCH ARTICLE OPEN ACCESS

Influence of the Chalcogen Anion on the Structural, Electronic, Phonon, Thermal, and Optical Properties of Yttrium Hydride Chalcogenides Material YHX (X = S, Se, and Te): A First-Principles Study

Tadesse Bekele Aredo[1] | Adem Beriso Bejo[2] | Melak Birara Dagnew[3] | Muhidin Mudi Gemeda[1] | Dessalegn Olkeba Furi[4]

[1]Department of Physics, College of Natural and Computational Sciences, Bule Hora University, Bule Hora, P.O. Box 144, Ethiopia | [2]Department of Physics, College of Natural and Computational Science, Madda Walabu University, Bale Robe, P.O. Box 247, Ethiopia | [3]Department of Physics, College of Natural and Computational Sciences, Injibara University, Injibara, P.O. Box 40, Ethiopia | [4]Action Against Hunger Organization, Addis Ababa, P.O. Box 2357, Ethiopia

Correspondence: Tadesse Bekele Aredo (tadesseb154@gmail.com)

Received: 17 April 2026 | **Revised:** 29 June 2026 | **Accepted:** 27 July 2026

Academic Editor: Sefer Bora Lisesivdin

Keywords: chalcogen substitution | density functional theory | optoelectronic materials | phonon dispersion | spin–orbit coupling | yttrium hydrogen chalcogenides

ABSTRACT

The structural, electronic, vibrational, optical, and thermodynamic properties of yttrium hydrogen chalcogenides (YHS, YHSe, and YHTe) are systematically investigated using first-principles density functional theory (DFT), with phonon and thermodynamic properties determined using Phonopy calculations. All compounds are dynamically stable, exhibiting progressive lattice expansion from YHS to YHTe due to increasing chalcogen atomic size. Additionally chalcogen substitution effectively tunes the electronic structure by modulating the band gap and density of states (DOS) through enhanced hybridization between Y-d and chalcogen-p orbitals. Spin–orbit coupling (SOC) introduces subtle yet non-negligible modifications, with stronger effects observed for heavier chalcogens Te-based systems. The band gaps show slight SOC-induced variations, changing from 1.6385 to 1.6472 eV for YHS, 1.5152 to 1.5172 eV for YHSe, and from 1.52 to 1.42 eV for YHTe, reflecting enhanced relativistic effects in Te-based systems. YHS and YHSe retain indirect band gaps semiconductor, whereas YHTe exhibits a robust direct band gap semiconductor. Phonon dispersion confirms dynamical stability and reveals systematic softening of vibrational modes from YHS to YHTe, attributed to increased atomic mass and reduced interatomic force constants. This behavior correlates with enhanced electronic polarizability and modified bonding. Optical properties exhibit a red shift in the absorption edge with increased dielectric response. Thermodynamic analysis shows that entropy and specific heat increase with temperature, while Helmholtz free energy decreases and becomes more negative from YHS to YHTe, indicating improved thermodynamic stability. These findings highlight yttrium hydrogen chalcogenide compounds as promising tunable materials for optoelectronic and energy applications.

1 | Introduction

Chalcogen elements, including oxygen (O), sulfur (S), selenium (Se), tellurium (Te), and polonium (Po), are members of group 16 of the periodic table and are characterized by an outer electronic configuration of nS^2np^4. Owing to their distinctive chemical flexibility, these elements participate in the formation of a broad

This is an open access article under the terms of the Creative Commons Attribution License, which permits use, distribution and reproduction in any medium, provided the original work is properly cited.

Copyright © 2026 Tadesse Bekele Aredo et al. *Advances in Condensed Matter Physics* published by John Wiley & Sons Ltd.

range of compounds, such as oxides, sulfides, selenides, and tellurides, which are widely recognized as important ore-forming materials [1]. Their exceptional ability to establish diverse chemical bonds and generate various compound structures makes them highly significant in materials science. According to periodic trends, the physicochemical characteristics of chalcogen elements are governed by their atomic structures and evolve systematically with increasing atomic numbers rather than occurring randomly. The unique chemical behavior of chalcogens has enabled the development of numerous technologically important materials with applications across various fields [2]. A key feature of chalcogen-based compounds is their capacity to exhibit multiple bonding configurations and oxidation states, providing opportunities to tailor their structural, electronic, optical, and thermal characteristics for specific applications [3]. Furthermore, recent progress in computational materials science has demonstrated that chalcogen-containing materials offer significant potential for engineering advanced multifunctional systems by precisely controlling their electronic structures and related physical properties through first-principles theoretical approaches [4]. In recent years, chalcogenide-based materials have gained considerable research interest owing to their distinctive physicochemical characteristics and broad potential in advanced technological fields, such as photovoltaic systems, thermoelectric devices, phase-change memory technologies, optoelectronics, and superconducting applications. Selenium- and tellurium-containing compounds have demonstrated promising capabilities for use in semiconductor components, transistor technologies, and radiation detection devices [5]. Recent review articles have further highlighted the outstanding potential of chalcogenide materials for energy conversion applications, especially in thermoelectric and photovoltaic technologies, as a result of their tunable electronic structures, efficient charge transport properties, and strong optical absorption behavior [4]. Moreover, their covalent bonding characteristics, moderate band gap energies, and high optical absorption coefficients contribute to their suitability for a variety of energy-related and electronic device applications [6].

Importantly, the properties of these materials are highly sensitive to compositional modifications, especially through chalcogen substitution, which provides an effective strategy for tailoring the material performance. Chalcogen substitution involves replacing one chalcogen atom with another, leading to systematic variations in the atomic size, electronegativity, and polarizability [7]. These changes directly influence lattice parameters, bonding characteristics, and the electronic structure. For example, substitution from lighter to heavier chalcogens typically results in lattice expansion and enhanced spin–orbit coupling (SOC), which significantly affects the band structure and optical response [6, 7]. Recent first-principles studies have demonstrated that chalcogen substitution can significantly modify band dispersion, density of states (DOS), and carrier effective mass, thereby enabling precise tuning of electronic properties [8].

From an electronic perspective, chalcogen substitution can effectively tune the band gap and carrier transport properties. For instance, selenium substitution has been reported to enhance charge delocalization and electrical conductivity in conjugated systems, thereby improving the thermoelectric performance [9]. Furthermore, advanced studies have shown that substitution-induced orbital hybridization plays a crucial role in enhancing charge transport and optimizing thermoelectric efficiency [8]. Moreover, the substitution process can introduce localized states or alter hybridization between orbitals, leading to significant modifications in the DOS and optical transitions.

In addition to electronic and structural effects, chalcogen substitution strongly influences phonon dynamics and thermal properties. The variation in atomic mass and bonding strength affects phonon dispersion and lattice vibrations, which are critical for thermal conductivity and superconductivity. For example, doping or substitution in chalcogenide glasses alters crystallization kinetics and activation energies, demonstrating the sensitivity of thermal behavior to compositional changes [5].

Recent investigations reveal that mass fluctuation and lattice disorder induced by chalcogen substitution significantly reduce the lattice thermal conductivity by enhancing phonon scattering mechanisms [8]. Such phonon engineering strategies are essential for improving the thermoelectric performance and controlling heat transport in advanced functional materials. Overall, chalcogen substitution has emerged as a powerful and versatile approach for engineering advanced functional materials. By systematically varying the chalcogen species, it is possible to achieve precise control over structural, electronic, optical, and thermal properties, enabling the optimization of materials for next-generation technological applications. Consequently, state-of-the-art first-principles calculations combined with materials informatics are increasingly used to predict and design high-performance chalcogenide systems with tailored functionalities [4, 8]. Despite the growing interest in chalcogenide-based materials, systematic studies of yttrium hydrogen chalcogenides remain scarce. Existing investigations have primarily focused on individual compounds or specific external effects such as pressure and doping, while the influence of varying the chalcogen species across the YHX (X = S, Se, and Te) series has received limited attention [10]. Since the chalcogen atom plays a crucial role in determining bonding characteristics, electronic structure, optical response, and lattice dynamics, a comparative investigation of the YHX series is essential for understanding composition property relationships. Such knowledge is important for assessing the suitability of these materials for applications in optoelectronic, thermoelectric, and energy-conversion devices [11–13].

Although previous studies have extensively explored the effects of pressure and elemental doping on YHSe and related materials, systematic investigations of chalcogen substitution across the series YHX (X = S, Se, and Te) remain limited. Understanding how such substitutions affect structural stability, electronic band characteristics, phonon dispersion, and thermal conductivity is essential for the rational design of advanced functional materials. In this work, we employ first-principles calculations to systematically investigate the influence of the chalcogen anion on the structural, electronic, phonon, optical, and thermal properties of YHX (X = S, Se, and Te). By varying the substituting element (S, Se, and Te), we aim to reveal the underlying mechanisms governing property modulation. The outcomes of this study are expected to provide valuable insights into chalcogenide material engineering and contribute to the development of next-generation materials for energy and electronic applications.

2 | Theoretical Background and Computational Details

2.1 | Theoretical Background

The Kramers–Kronig relations describe the fundamental connection between the real and imaginary parts of a complex response function, such as the dielectric function. They are based on the principle of causality and allow one part to be determined from the other through integral transformations over frequency [14].

$$\varepsilon(\omega) = \varepsilon_1(\omega) + i\varepsilon_2(\omega). \tag{1}$$

The real part of the dielectric function, $\varepsilon_1(\omega)$, is obtained from the Kramers–Kronig relations, which establish a connection between the real and imaginary components of a frequency-dependent response function.

$$\varepsilon_1 = 1 + \frac{2p}{\pi}\int_0^{\infty} \frac{\omega'\ \varepsilon_2(\omega)\ d\omega'}{\omega'^2 - \omega^2}, \tag{2}$$

where p represents the Cauchy principal value, ω is the frequency of incident radiation, ω' represents a variable of integration over the entire frequency range of the material's response, and $\varepsilon_2(\omega)$ is the complex component of the dielectric function, defined as follows:

$$\varepsilon_2(\omega) = \sqrt{\frac{m^2\omega^2}{4e^2\pi^2}}\sum_n \int_0^{\infty} \upsilon\ |M|\ c^2 f_n(1 - f_n)\delta(E_C - E_V - E_n)\ d^3k. \tag{3}$$

The parameters e, ω, m, c, υ, M, and k denote the elementary charge, the frequency of the incident radiation, the electron rest mass, the speed of light, the single-particle velocity operator, the dipole matrix elements, and the momentum vector, respectively. The term f_n represents the Fermi–Dirac distribution for the n^{th} state.

The function $\delta(E_C - E_V - E_n)$ corresponds to the Dirac delta function, evaluated at the energy difference between the conduction band edge, valence band edge, and a specific electron-state energy. Here, E_C, E_V, and E_n refer to the conduction band minimum (CBM), valence band maximum (VBM), and the energy of the electron state, respectively. Equation (3) describes the average electronic transitions from occupied valence band states to unoccupied conduction band states at a fixed k-point integrated over the Brillouin zone. A detailed understanding of both the real and imaginary parts of the dielectric function enables the evaluation of key optical properties such as the refractive index $n(\omega)$, absorption coefficient, reflectivity, extinction coefficient, electron energy loss function (ELF), and optical conductivity. Furthermore, the real and imaginary components of the dielectric function are directly used to determine the real part of the refractive index, $n(\omega)$ as follows:

$$n(\omega) = \frac{1}{\sqrt{2}}\sqrt{\sqrt{\varepsilon_1^2 + \varepsilon_2^2} + \varepsilon_1}. \tag{4}$$

The imaginary part of the refractive index, $\kappa(\omega)$, can be expressed in terms of the dielectric function components as follows:

$$\kappa(\omega) = \frac{1}{\sqrt{2}}\sqrt{\sqrt{\varepsilon_1^2 + \varepsilon_2^2} - \varepsilon_1}. \tag{5}$$

The photon frequency, ω, which governs the material's absorption, is related to the absorption coefficient, $\alpha(\omega)$, and can be expressed as follows:

$$\alpha(\omega) = \sqrt{2\omega}\sqrt{\sqrt{\varepsilon_1^2 + \varepsilon_2^2} - \varepsilon_1}. \tag{6}$$

The electron ELF, $L(\omega)$, which describes the energy lost by fast electrons traversing a material, is expressed in terms of the dielectric function as follows:

$$L(\omega) = \frac{\varepsilon_2(\omega)}{\varepsilon_1^2(\omega) + \varepsilon_2^2(\omega)}. \tag{7}$$

2.2 | Computational Details

All calculations were carried out using density functional theory (DFT) as implemented in the Quantum ESPRESSO package [15], combined with the Phonopy code for phonon dispersion and thermal property calculations [16]. A plane-wave basis set was employed with a kinetic energy cutoff of 120 Ry, and the Brillouin zone was sampled using a $12 \times 12 \times 12$ Monkhorst–Pack k-point mesh after careful convergence testing. Structural optimization was performed using the Broyden–Fletcher–Goldfarb–Shanno (BFGS) algorithm until the total energy, atomic forces, and stresses were minimized within predefined convergence thresholds. The exchange–correlation interactions were treated using the generalized gradient approximation in the Perdew–Burke–Ernzerhof (PBE) functional [17]. SOC effects were included to account for relativistic interactions, particularly for systems containing heavier chalcogen elements, Te. The SOC calculations were performed within a fully relativistic, noncollinear framework, providing a more accurate description of the electronic band structure [18, 19]. Electronic and optical properties were calculated based on the converged ground-state structure, where the frequency-dependent dielectric function was obtained within the framework of the linear response theory. A denser k-point mesh was used for the accurate evaluation of the electronic DOS and optical spectra. All calculations were performed within a non-spin-polarized framework, assuming nonmagnetic ground states for all compounds.

3 | Results and Discussion

3.1 | Structural Properties

The optimized lattice parameters of the YHX (X = S, Se, and Te) compounds exhibit a clear and systematic dependance on chalcogen substitution. Figure 1 presents the optimized crystal structures of (a) YHS, (b) YHSe, and (c) YHTe, illustrating the structural evolution with chalcogen substitution. YHS crystallizes with optimized lattice constants of $a = b = 3.73$ Å and $c = 3.72$ Å. Upon substituting S with Se, the lattice expands to $a = b = 3.81$ Å and $c = 3.87$ Å for YHSe, in good agreement with the corresponding experimental values of $a = 3.83$ Å and $c = 3.88$ Å [10]. Further substitution with Te results in a larger unit cell, with optimized lattice constants $a = b = 3.97$ Å and $c = 4.19$ Å

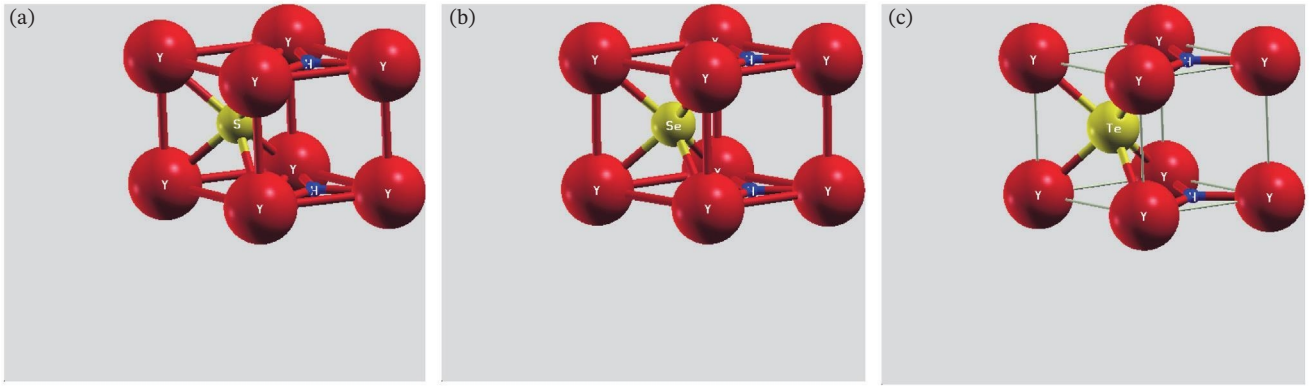


FIGURE 1 | Crystal structures of (a) YHS, (b) YHSe, and (c) YHTe showing the chalcogen substitution effect on the structure.

for YHTe. This systematic increase in the lattice parameters from YHS to YHTe is attributed to the progressive increase in the ionic (or covalent) radius of the chalcogen atom, which weakens the Y–X bonding and leads to lattice expansion. This trend is consistent with previous reports on transition metal dichalcogenides [7]. Moreover, the calculated bond angles and bond lengths vary systematically with chalcogen substitution. The Y–S–Y bond angle is 81.65°, which increases to 82.81° for Y–Se–Y and further to 84.78° for Y–Te–Y. The Y–S, Y–Se, and Y–Te bond lengths are 2.84, 2.93, and 3.11 Å respectively, reflecting the increasing atomic radius of the chalcogen atoms. The Y–H bond length remains nearly constant at 2.15 Å for YHS and YHSe, while it increases slightly to 2.29 Å for YHTe. Furthermore, the S–Y–H, Se–Y–H, and Te–Y–H bond angles are 67.77°, 67.97°, and 68.30°, respectively. These structural variations demonstrate the significant influence of chalcogen substitution on the geometric characteristics of the YHX compound. This observed behavior is in good agreement with previous studies reported in the literature [20]. This monotonic expansion of the lattice is primarily attributed to the progressive increase in the atomic radius from sulfur to tellurium. The enlargement of the lattice parameters reflects the incorporation of heavier and larger chalcogen atoms, which leads to an increase in interatomic distances. This trend is consistent with the periodic nature of Group 16 elements, where the atomic size and polarizability increase down the group. As a result, the crystal structure becomes more expanded and slightly less rigid when moving from YHS to YHTe, which is in good agreement with previous studies [20, 21]. A closer examination of the lattice geometry reveals that while the in-plane parameters ($a = b$) increase moderately, the out-of-plane lattice constant (c) shows a more pronounced increase, particularly for YHTe. This leads to a gradual increase in the c/a ratio, indicating anisotropic lattice expansion. Such anisotropy suggests that the bonding environment along the c-direction is more sensitive to chalcogen substitution, possibly due to directional differences in the orbital overlap and bonding character. The increase in lattice volume across the series also implies a reduction in packing density and enhanced structural flexibility in YHTe compared to that in YHS. This behavior can significantly influence other physical properties, including vibrational dynamics and electronic structure, by modifying the overlap between atomic orbitals. The systematic increase in lattice parameters and the c/a ratio reflects the strong influence of atomic size and bonding characteristics, with YHTe showing the most expanded and anisotropic structure, whereas YHS retains a more compact and rigid lattice. This observed behavior is consistent with previously reported studies on chalcogenides [20, 21].

3.2 | Electronic Properties

The electronic band structures of YHS, YHSe, and YHTe reveal that all three compounds exhibit semiconducting behavior, with a systematic modulation of the band gap upon chalcogen substitution. Figure 2a–c illustrates the electronic band structures along with the corresponding projected DOS (PDOS) for the chalcogen substitution cases. When SOC is included, the calculated band gaps are 1.6472 eV for YHS, 1.5172 eV for YHSe, and 1.42 eV for YHTe, compared to 1.6385, 1.5152, and 1.52 eV, respectively, without SOC. This indicates that SOC has a negligible effect on YHS and YHSe, whereas it induces a noticeable reduction in the band gap of YHTe due to the stronger relativistic effects associated with the heavier Te atom. This behavior is in good agreement with previous studies on chalcogen substitutions [7, 22]. The overall trend shows that the band gap decreases from YHS to YHSe, followed by a further reduction in YHTe when the SOC is considered. This behavior indicates that the electronic structure is highly sensitive to the atomic size, electronegativity, and orbital characteristics of the chalcogen atoms. Notably, the reduction of band gap and an indirect-to-direct band gap semiconductor transition is observed, which is in good agreement with previous studies on the effects of chalcogen substitution [23]. The observed trend can be attributed to the progressive enhancement of p-orbital delocalization and increased hybridization between the Y-d and X-p (X = S, Se, and Te) states as the atomic number of the chalcogen increases. The band gap decreases systematically with heavier chalcogen substitution, which is in good agreement with previous studies on chalcogen-substituted materials [24].

In particular, heavier chalcogen elements such as Te introduce stronger SOC and lead to broader valence bands, which contribute to band gap narrowing and enhanced band dispersion. This trend is in good agreement with previous studies on chalcogen substitution effects [22]. As shown in Figure 2a–c, the PDOS indicates that the VBM is predominantly composed of chalcogen p-states, while the CBM is mainly derived from Y-states. The substitution from S to Te increases the orbital overlap and reduces the energy separation between these states, thereby facilitating electronic transitions.

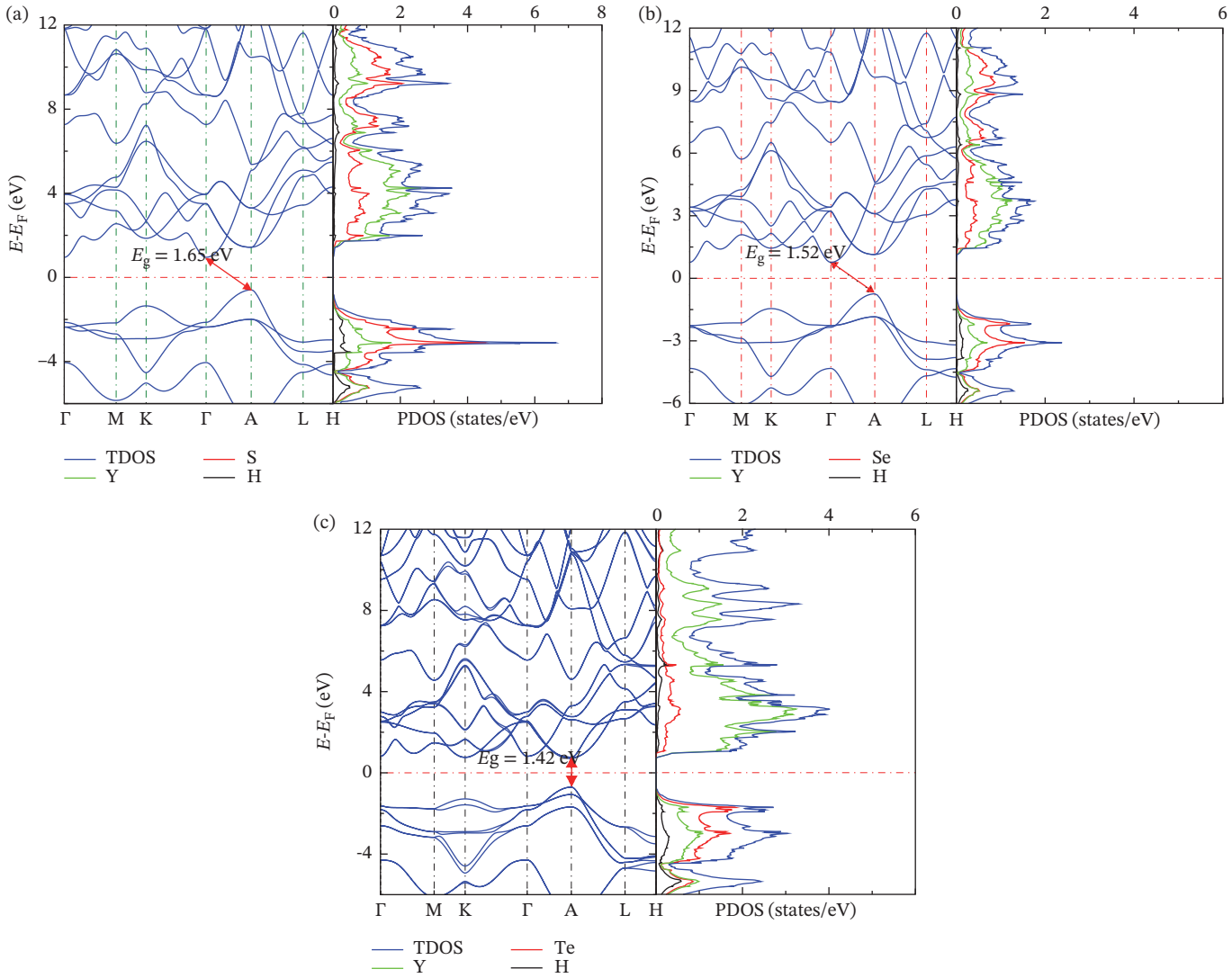


FIGURE 2 | Electronic band structures along high-symmetry directions including spin–orbit coupling (SOC), along with the corresponding partial density of states (PDOS) for (a) YHS, (b) YHSe, and (c) YHTe.

Moreover, YHS and YHSe exhibit indirect band gap semiconductors, while YHTe shows a direct band gap nature. This transition from an indirect to a direct band gap with increasing chalcogen atomic number highlights the strong sensitivity of the electronic structure to chemical substitution. This trend is consistent with previous studies on chalcogen substitution [23].

3.3 | Phonon Properties

The phonon dispersion curves presented in the figure confirm the dynamical stability of all three systems (YHS, YHSe, and YHTe) as no imaginary frequencies are observed throughout the Brillouin zone. Figure 3a–c presents the phonon dispersion relations along the high-symmetry directions, together with the corresponding phonon partial DOS and total phonon DOS (TDOS) for the chalcogen-substituted systems. A clear trend is observed with chalcogen substitution as we move from YHS to YHTe, and the phonon frequencies systematically shift toward lower values. This behavior is primarily attributed to the increase in atomic mass from sulfur to tellurium, which reduces the vibrational frequencies according to lattice dynamics principles. This trend is consistent with previous studies on chalcogen substitution effects [25]. Consequently, YHTe exhibits the softest phonon modes, while YHS shows relatively higher-frequency vibrations. Additionally, the phonon band structure reveals a progressive narrowing of the phonon bandwidth from YHS to YHTe, indicating weaker bonding strength and enhanced lattice softness in heavier chalcogen systems. Furthermore, the increased phonon density at lower frequencies in YHTe suggests a higher contribution to vibrational entropy, which is consistent with the observed thermodynamic trends in this study. The phonon dispersion further supports these findings by demonstrating a clear mass-dependent softening of vibrational modes from YHS to YHTe. The absence of imaginary frequencies confirms dynamical stability, while the shift of phonon branches toward lower frequencies in YHTe reflects weaker interatomic bonding and increased lattice anharmonicity.

3.4 | Optical Properties

3.4.1 | Dielectric Function

From an optical perspective, these phonon-induced structural and electronic modifications strongly influence the dielectric

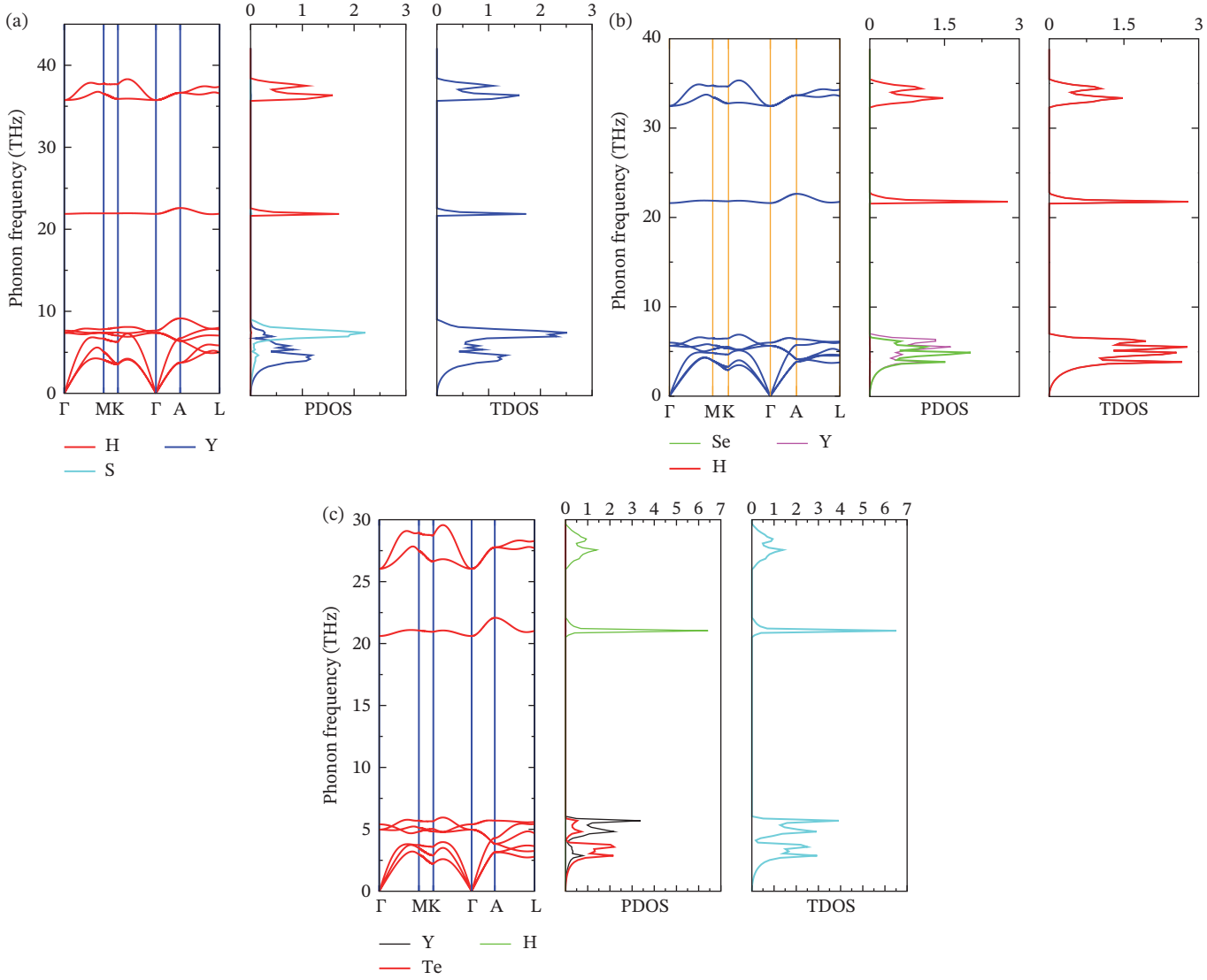


FIGURE 3 | Phonon dispersion relations along high-symmetry directions, along with the phonon partial density of states (PDOS) and total phonon density of states (TDOS) for (a) YHS, (b) YHSe, and (c) YHTe.

response and related optical parameters. The substitution of heavier chalcogen atoms leads to enhanced electronic polarizability, which results in an increase in the real part of the dielectric function. At the same time, the imaginary part of the dielectric function, which represents interband electronic transitions, shows noticeable shifts in peak positions toward lower photon energies from YHS to YHTe. This red-shift behavior is directly correlated with the reduction in band gap and the modification of electronic band dispersion due to chalcogen substitution. Moreover, the absorption spectra indicate that YHTe exhibits stronger absorption in the lower-energy (visible) region than that of YHS and YHSe. This enhanced visible-light absorption, together with its narrower direct band gap, indicates that YHTe is a more promising candidate for optoelectronic and photovoltaic applications. The enhanced optical response in heavier chalcogen systems can also be linked to stronger SOC effects, which become more pronounced with the increasing atomic number. The real part of the dielectric function shows an increasing trend from YHS to YHTe, indicating enhanced electronic polarizability in heavier chalcogen systems. The real part of the dielectric function, $\varepsilon_1(\omega)$, exhibits a clear dependance on both photon energy and chalcogen substitution. Figure 4 shows the real part of the dielectric function, $\varepsilon_1(\omega)$, as a function of photon energy for YHS, YHSe, and YHTe, illustrating the effect of chalcogen substitution on the optical response and the systematic enhancement of electronic polarizability with increasing chalcogen atomic number.

At zero photon energy ($\omega = 0$ eV), the static dielectric constant increases systematically from YHS (14.55) to YHSe (16.06) and further to YHTe (23.28), indicating an enhanced electronic polarizability with increasing chalcogen atomic number. This trend is mainly attributed to the increased lattice constant, stronger orbital hybridization, and enhanced SOC effects in heavier chalcogen systems. The observed increase in both the static (zero-frequency) dielectric constant and the imaginary part of the dielectric function with chalcogen substitution is consistent with previously reported results [20, 23]. The maximum peak values of the real part of the dielectric function are 42.6 at 2.34 eV for YHS, 46.13 at 2.08 eV for YHSe, and 56.25 at 1.42 eV for YHTe. The systematic red shift of the peak position from YHS to YHTe reflects the reduction in band gap and enhanced

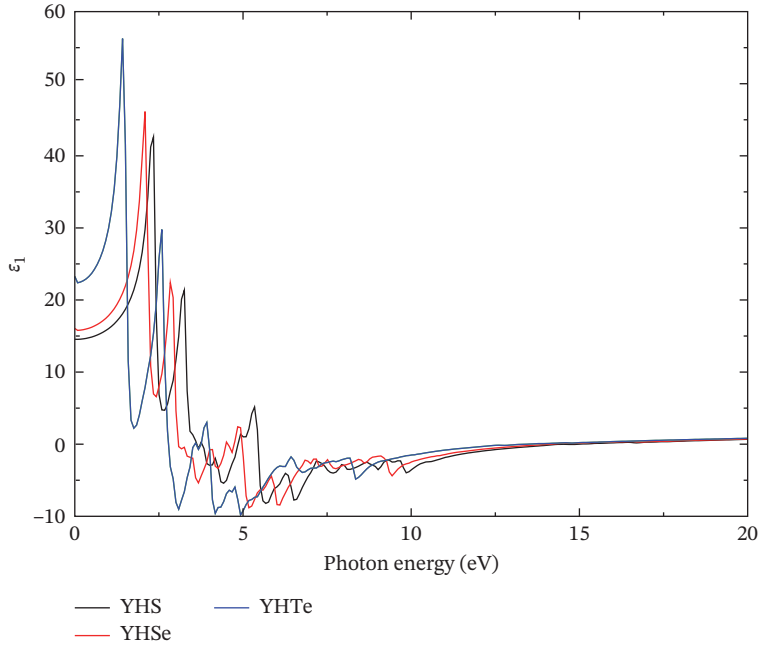


FIGURE 4 | Real part of the dielectric function, $\varepsilon_1(\omega)$, as a function of photon energy for YHS, YHSe, and YHTe, illustrating the effect of chalcogen substitution on the optical response.

interband transition probability due to chalcogen substitution. The increase in peak intensity further confirms strengthened light–matter interaction and improved optical response in heavier chalcogen-based systems, particularly YHTe, which exhibits the most pronounced dielectric activity. This trend is consistent with previous studies [23].

Figure 5 shows the imaginary part of the dielectric function, $\varepsilon_2(\omega)$, as a function of photon energy for YHS, YHSe, and YHTe, illustrating the effect of chalcogen substitution on the optical response and the systematic enhancement of optical absorption with increasing chalcogen atomic number. The imaginary part of the dielectric function, $\varepsilon_2(\omega)$, exhibits a pronounced red shift of optical peaks with increasing chalcogen atomic number, corresponding to reduced interband transition energies due to band gap narrowing. This behavior is consistent with electronic band structure analysis and highlights the strong correlation between electronic states and optical transitions. The magnitude of $\varepsilon_2(\omega)$ also increases systematically with chalcogen substitution, indicating enhanced optical absorption and stronger interband transition probabilities. The peak values of the imaginary part of the dielectric function are 42.07 at 2.42 eV for

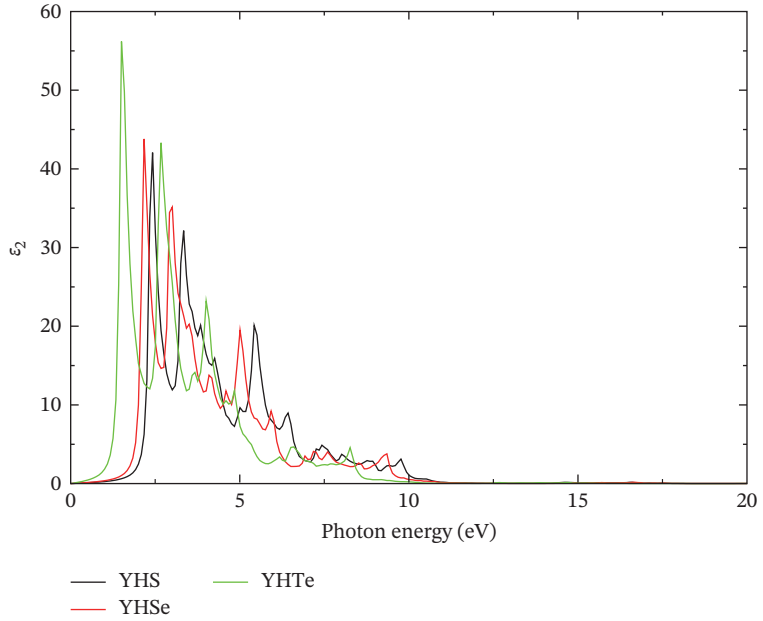


FIGURE 5 | Imaginary part of the dielectric function, $\varepsilon_1(\omega)$, as a function of photon energy for YHS, YHSe, and YHTe, illustrating the effect of chalcogen substitution on the optical response.

YHS, 43.81 at 2.13 eV for YHSe, and 56.18 at 1.50 eV for YHTe. This clear red shift and intensity enhancement confirm that heavier chalcogen incorporation significantly improves light–matter interaction, with YHTe exhibiting the strongest optical response among the studied compounds. This trend is consistent with previous reports on transition metal dichalcogenides where a systematic red shift in optical absorption is observed from sulfides to selenide and tellurides due to chalcogen substitution [24].

The absorption spectra further reveal that YHTe exhibits superior optical absorption in the visible region, whereas YHS shows stronger absorption in the higher energy region. This systematic shift in the absorption edge is particularly important for optoelectronic applications as it demonstrates that chalcogen substitution provides an effective strategy for tailoring the spectral response of the material. The observed enhancement in absorption intensity for YHTe can be attributed to increased interband transition probabilities arising from stronger orbital hybridization between Y-d and chalcogen p states as well as enhanced SOC effects in heavier chalcogen elements. Consequently, these results highlight the strong tunability of optical properties in YHX compounds through controlled chalcogen substitution, enabling targeted optimization for optoelectronic and energy-related applications.

Another critical aspect is the role of SOC, which becomes increasingly significant from S to Te due to the increasing atomic number. SOC induces noticeable band splitting near high-symmetry points and modifies the band curvature, thereby influencing the effective masses of charge carriers. This effect is particularly pronounced in YHTe, where the stronger relativistic interaction associated with Te atoms leads to improved optical response, reduced band gap, and enhanced light–matter interaction compared to that in YHS and YHSe. This trend is consistent with the previous study of chalcogen substitution effects [20, 26, 27].

3.4.2 | Electron ELF

In the present study, the ELF spectra of YHS, YHSe, and YHTe exhibit well-defined peaks corresponding to plasmon resonance frequencies, which arise from collective oscillations of valence electrons. Figure 6 presents the electron ELF as a function of the photon energy. The intensity of the loss peaks increases for heavier chalcogens, particularly YHSe, in the photon energy range of 10–20 eV, reflecting stronger electron energy-loss processes in this region for all compounds, along with a clear red shift from YHS to YHTe. The observed behavior is consistent with the trends in the dielectric function and optical absorption, as shown in the imaginary part of the dielectric function, confirming that chalcogen substitution in the 10–20 eV energy range leads to reduced optical absorption. This trend is in good agreement with previous theoretical studies on chalcogen-substituted materials [28].

3.5 | Thermal Properties

The temperature-dependent variations of the specific heat at constant volume, entropy, and Helmholtz free energy for the YHS, YHSe, and YHTe systems are evaluated within the harmonic approximation using the calculated phonon frequencies. Figure 7 presents the effect of chalcogen substitution on the entropy of yttrium chalcogen systems. As described in Figure 7, at absolute zero temperature (0 K), the entropy becomes zero for YHS, YHSe, and YHTe systems, in agreement with previous reports [20, 29]. This reflects the fact that atoms occupy their equilibrium positions without vibrational disorder. At this temperature, entropy reaches its minimum value due to the absence of atomic thermal vibrations. As the temperature increases up to 1000 K, the entropy progressively increases due to intensified atomic vibrations and the resulting rise in thermal disorder for the three systems YHS, YHSe, and YHTe. At 1000 K, the entropy reaches approximately 130.43, 143.32, and 155.05 J/K/mol for the YHS,

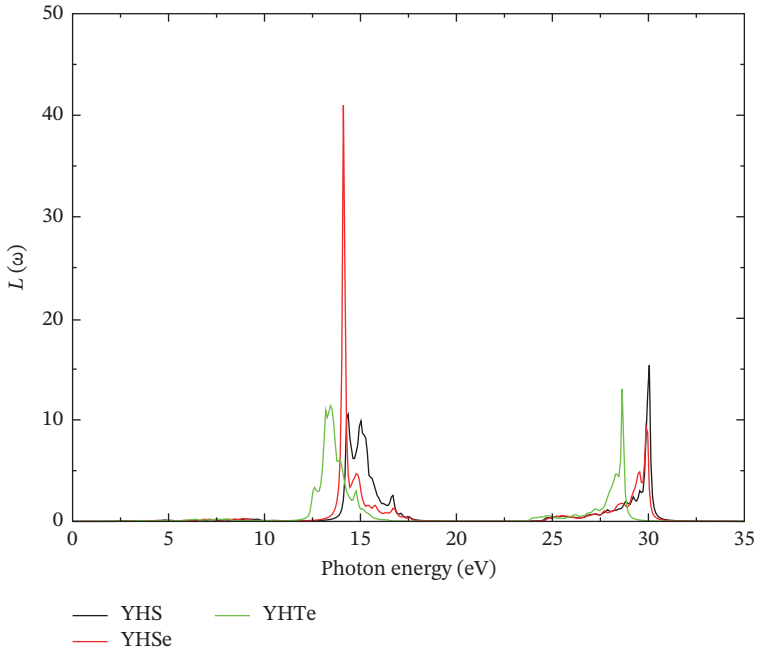


FIGURE 6 | Electron energy loss function, $L(\omega)$, as a function of photon energy for YHS, YHSe, and YHTe, illustrating the effect of chalcogen substitution on the optical response.

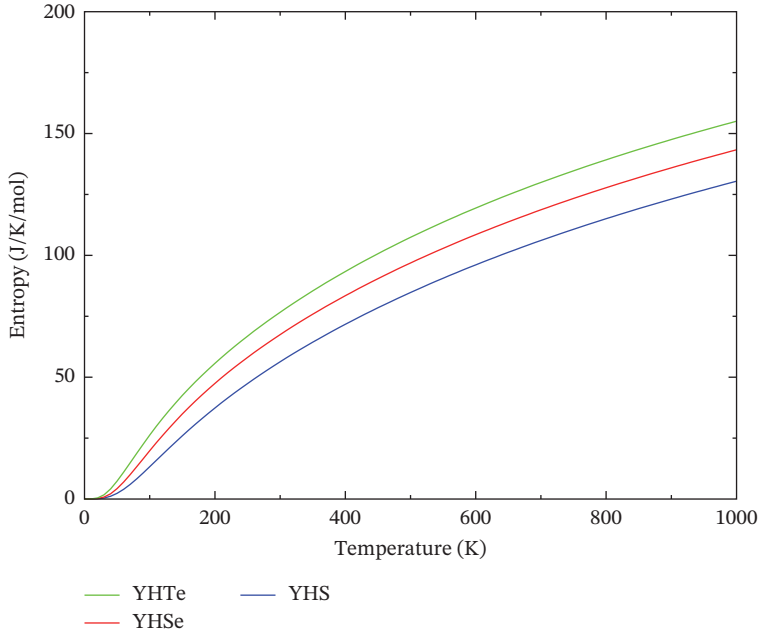


FIGURE 7 | Temperature dependance of entropy (S) for the YHS, YHSe, and YHTe systems.

YHSe, and YHTe systems, respectively. This trend indicates a systematic increase in entropy from YHS to YHTe at the same temperature (1000 K). The observed enhancement is attributed to the substitution of lighter sulfur atoms with heavier tellurium atoms, which leads to increased lattice vibrational disorder and a higher density of accessible phonon states.

The temperature dependance of the specific heat capacity (C_V) is also shown in Figure 8. At 0 K, C_V is zero for all three systems and progressively increases with increasing temperature, consistent with previous results reported in ref. [20, 29] as expected since no phonon modes are thermally excited at absolute zero. At 1000 K, the specific heat at constant volume reaches approximately 69.98, 70.66, and 71.72 J/K/mole for YHS, YHSe, and YHTe systems, respectively. The heat capacity at constant volume (C_v) increases with rising temperature for all systems (YHS, YHSe, and YHTe) and shows a systematic increase from YHS to YHTe at a given temperature. Figure 9 illustrates the temperature dependance of the Helmholtz free energy. The Helmholtz free energy attains its highest value at 0 K, reaching 26.46, 23.61, and 20.22 kJ/mol for YHS, YHSe, and YHTe, respectively. This indicates the maximum internal energy of the systems in the absence of significant thermal fluctuations, consistent with previous reports [29]. As the temperature increases, the Helmholtz free energy gradually decreases and becomes more negative, reaching minimum values of −50.32, −64.01, and −76.95 kJ/mol at 1000 K for the YHS, YHSe, and YHTe systems, respectively. This behavior is primarily attributed to the increasing contribution of the entropy term

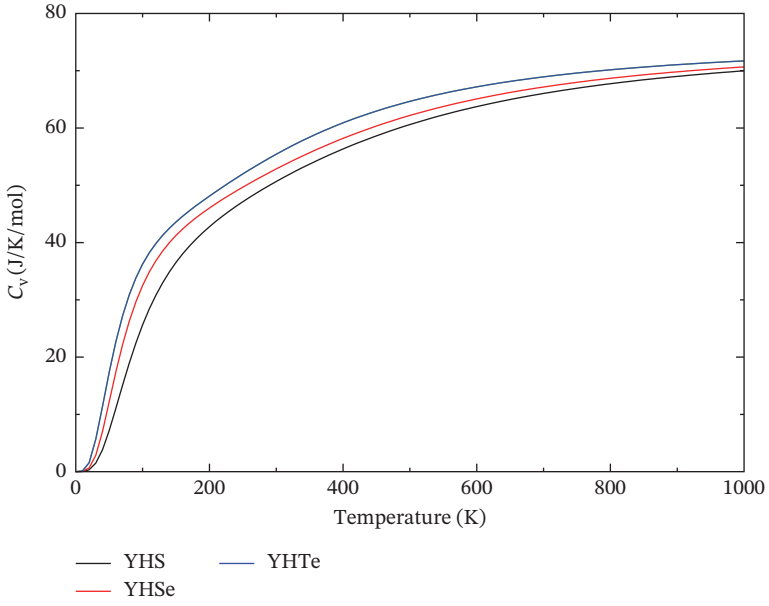


FIGURE 8 | Temperature dependance of the heat capacity at constant volume (C_v) for the YHS, YHSe, and YHTe systems.

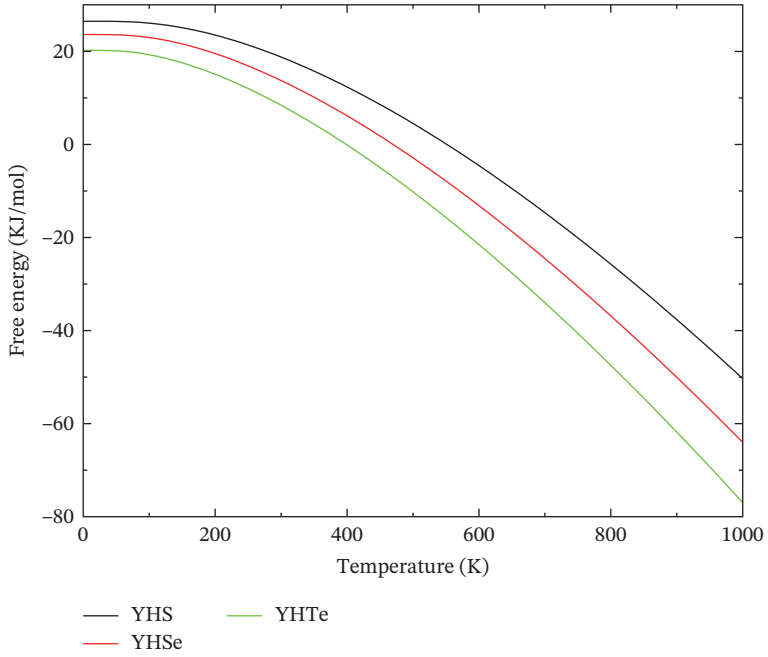


FIGURE 9 | Temperature dependance of the Helmholtz free energy (F) for the YHS, YHSe, and YHTe systems.

(−TS), which becomes dominant at elevated temperatures. The progressive decrease in free energy from YHS to YHTe indicates enhanced thermodynamic stability with the substitution of lighter sulfur atoms by selenium and heavier tellurium atoms over the entire temperature range of 0–1000 K. The calculated thermodynamic behavior is in good agreement with previously reported theoretical studies on ytterbium chalcogenides [20].

4 | Conclusion

In this work, first-principles DFT calculations were employed to systematically investigate the structural, electronic, phonon, optical, and thermal properties of yttrium hydrogen chalcogenides, YHX (X = S, Se, and Te). The results demonstrate that chalcogen substitution provides an effective approach for tuning the physical properties of these compounds. The optimized structures satisfy dynamical stability criteria, while the lattice parameters increase systematically from YHS to YHTe because of the larger atomic radius of the chalcogen atoms. Electronic structure calculations reveal semiconducting behavior for all compounds, with a progressive reduction in band gap from YHS to YHTe. The inclusion of SOC has only a minor effect on YHS and YHSe but produces a noticeable reduction in the band gap of YHTe. Moreover, the band gap character changes from indirect in YHS and YHSe to direct in YHTe, indicating the strong influence of chalcogen substitution on the electronic structure. The phonon calculations confirm the dynamical stability of all three compounds and show a systematic softening of phonon modes with the increasing chalcogen atomic mass. The optical properties exhibit a corresponding red shift in the absorption edge and enhanced dielectric response from YHS to YHTe, with YHTe showing the strongest absorption in the visible regions. Thermal calculations further indicate that entropy and heat capacity increase with temperature, whereas the Helmholtz free energy decreases, reflecting the expected thermodynamic behavior of these materials. Overall, the results demonstrate that chalcogen substitution enables systematic control of the structural, electronic, vibrational, optical, and thermal properties of the YHX family, providing useful insights into the design of hydrogen chalcogenide materials with tunable properties. Based on the calculated results, YHTe appears to be a promising candidate for future optoelectronic and photovoltaic applications because of its direct band gap and enhanced optical absorption, while YHS may be more suitable for applications requiring a wider band gap and greater structural rigidity. However, it should be noted that the present study is based entirely on first-principles calculations under ideal crystalline conditions. Experimental synthesis and characterization, together with more advanced theoretical investigations of temperature-dependent and defect-related effects, are required to validate and further extend the present predictions.

Author Contributions

All listed authors made substantial intellectual contribution to this work. Tadesse Bekele Aredo conceived the research, designed the study, performed all first principle calculations, analyzed and interpreted the computational results, prepared the figure, and wrote the original manuscript. Adem Beriso Bejo contributed to scientific discussion, interpretation of the results, critical revision of the manuscript, and improvement of the scientific content. Melak Birara Dagnew assisted with methodology, interpretation of computational findings, manuscript review, and language editing. Muhidin Mudi Gemeda contributed to validation of computational methods, discussion of the results, critical revision of the manuscript, and approval of the final version. Dessalegn Olkeba Furi contributed to scientific discussion, interpretations of the results, critical review of the manuscript, language editing, and improvement of the presentation of the manuscript.

Acknowledgments

The authors acknowledge the Ministry of Education (MoE), Ethiopia, for providing access to and support for the high-performance computing (HPC) facilities used in this study. Moreover, the authors used generating

AI solely to assist with language editing and improve the clarity and readability of the manuscript.

Funding

This research did not receive any specific grant from funding agencies in the public, commercial, or not-for-profit sectors.

Disclosure

All the authors critically revised the manuscript, approved the final version, and agree to be accountable for all aspects of the publication.

Conflicts of Interest

The authors declare no conflicts of interest.

Data Availability Statement

The data that support the findings of the study are available within the article.

References

1. H. Sicius, "Chalcogens: Elements of the Sixth Main Group," in *Handbook of the Chemical Elements*, ed. H. Sicius, (Springer, 2024): 351–401.

2. C. S. Clarke, D. A. Haynes, and J. M. Rawson, "Oxygen, Sulfur, Selenium, Tellurium and Polonium," *Annual Reports Section "A" (Inorganic Chemistry)* 104 (2008): 124–133.

3. N. P. Papoh, *Introductory Chapter: Chalcogen Chemistry – The Footprint into New Materials Development* (IntechOpen, 2019).

4. Y. Dan, Y. Zhao, X. Li, S. Li, M. Hu, and J. Hu, "Generative Adversarial Networks (GAN) Based Efficient Sampling of Chemical Composition Space for Inverse Design of Inorganic Materials," *npj Computational Materials* 6, no. 1 (2020): 84.

5. M. Rashad, N. M. Shaalan, A. A. l. Abd-Elmageed, R. Amin, M. M. Hafiz, and A. A. Abu-Sehly, "Extensive Thermal Study of Sulfur Dopants Effects on the Selenium Tellurium Glasses," *Journal of Non-Crystalline Solids* 558 (2021): 120630.

6. A. Chelh, B. Akenoun, S. Dahbi, et al., "Impact of Complete Sulfur Substitution by Selenium and Tellurium on the Structural, Electronic, Optical, and Photocatalytic Properties of CaAl2S4: A DFT Investigation," *Materials Today Communications* 48 (2025): 113377.

7. S. Manzeli, D. Ovchinnikov, D. Pasquier, O. V. Yazyev, and A. Kis, "2D Transition Metal Dichalcogenides," *Nature Reviews Materials* 2, no. 8 (2017): 17033.

8. W. Zhang, R. Mazzarello, M. Wuttig, and E. Ma, "Designing Crystallization in Phase-Change Materials for Universal Memory and Neuro-Inspired Computing," *Nature Reviews Materials* 4, no. 3 (2019): 150–168.

9. C. Chen, I. E. Jacobs, C. Jellett, et al., "Single Atom Selenium Substitution-Mediated P-Type Doping in Polythiophenes Toward High-Performance Organic Electronics and Thermoelectrics," *Advanced Electronic Materials* 8, no. 11 (2022): 2200053.

10. T. Schleid and H.-J. Meyer, "Hydrogen-Stabilized Yttrium Monoselenide," *Journal of Alloys and Compounds* 189, no. 1 (1992): 75–82.

11. F. Tesfaye and M. Moroz, "An Overview of Advanced Chalcogenide Thermoelectric Materials and Their Applications," *Journal of Electronic Research and Application* 2, no. 2 (2018): 28–41.

12. M. Channegowda, R. Mulla, Y. Nagaraj, et al., "Comprehensive Insights Into Synthesis, Structural Features, and Thermoelectric Properties of High-Performance Inorganic Chalcogenide Nanomaterials for Conversion of Waste Heat to Electricity," *ACS Applied Energy Materials* 5, no. 7 (2022): 7913–7943.

13. S. Puthran, G. S. Hegde, and A. N. Prabhu, "Review of Chalcogenide-Based Materials for Low-, Mid-, and High-Temperature Thermoelectric Applications," *Journal of Electronic Materials* 53, no. 10 (2024): 5739–5768.

14. J. D. Jackson, *Classical Electrodynamics* (John Wiley & Sons, Inc., 1999): 5.

15. P. Giannozzi, S. Baroni, N. Bonini, et al., "QUANTUM ESPRESSO: A Modular and Open-Source Software Project for Quantum Simulations of Materials," *Journal of Physics: Condensed Matter* 21, no. 39 (2009): 395502.

16. A. Togo and I. Tanaka, "First Principles Phonon Calculations in Materials Science," *Scripta Materialia* 108 (2015): 1–5.

17. J. P. Perdew, K. Burke, and M. Ernzerhof, "Generalized Gradient Approximation Made Simple," *Physical Review Letters* 77, no. 18 (1996): 3865–3868.

18. P. Giannozzi, O. Andreussi, T. Brumme, et al., "Advanced Capabilities for Materials Modelling With Quantum ESPRESSO," *Journal of Physics: Condensed Matter* 29, no. 46 (2017): 465901.

19. A. Dal Corso, "Projector Augmented-Wave Method: Application to Relativistic Spin-Density Functional Theory," *Physical Review B* 82, no. 7 (2010): 75116.

20. L. A. Eressa and Z. D. Gerbi, "Electronic, Elastic, Optical, and Thermodynamic Properties Study of Ytterbium Chalcogenides Using Density Functional Theory," *Advances in Condensed Matter Physics* 2024 (2024): 6646885.

21. A. Obeidat, S. Abu-Rajouh, and M.-K. Qaseer, "DFT Study of the Influence of Chalcogen Substitution on the Structural, Mechanical, Thermodynamic, Magnetic, and Electronic Properties of Ag_3FeX_4 (X = S, Se, Te)," *Chemical Physics* 598 (2025): 112857.

22. S. M. Alay-e-Abbas, N. Sabir, Y. Saeed, and A. Shaukat, "First-Principles Study of Structural and Electronic Properties of Alkali Metal Chalcogenides: M CH [M: Li, Na, K, Rb; CH: O, S, Se, Te]," *International Journal of Modern Physics B* 25, no. 29 (2011): 3911–3925.

23. Naeemullah, G. Murtaza, R. Khenata, A. Safeer, Z. A. Alahmed, and S. Bin Omran, "Shift of Band Gap From Indirect to Direct and Optical Response of CaO by Doping S, Se, Te," *Computational Materials Science* 91 (2014): 43–49.

24. K. F. Mak and J. Shan, "Photonics and Optoelectronics of 2D Semiconductor Transition Metal Dichalcogenides," *Nature Photonics* 10, no. 4 (2016): 216–226.

25. G. P. Srivastava, H. M. Tütüncü, and N. Günhan, "First-Principles Studies of Structural, Electronic, and Dynamical Properties of Be Chalcogenides," *Physical Review B* 70, no. 8 (2004): 85206.

26. M. P. Nowak and B. Szafran, "Spin Polarization Anisotropy in a Narrow Spin–Orbit-Coupled Nanowire Quantum Dot," (2018): 1–7.

27. Z. Y. Zhu, Y. C. Cheng, and U. Schwingenschlögl, "Giant Spin–Orbit-Induced Spin Splitting in Two-Dimensional Transition-Metal Dichalcogenide Semiconductors," *Physical Review B* 84, no. 15 (2011).

28. I. Zorić, M. Zäch, B. Kasemo, and C. Langhammer, "Gold, Platinum, and Aluminum Nanodisk Plasmons: Material Independence, Subradiance, and Damping Mechanisms," *ACS Nano* 5, no. 4 (2011): 2535–2546.

29. M. B. Dagnaw, A. Belay, K. H. Habura, G. B. Kassahun, U. Sherefedin, and G. A. Desalegn, "Ab Initio Calculations of Structural, Phonon, Thermal, Electronic, and Optical Properties of WxMo1−xS2ySe2 (1−y) Materials for x = 0, 0.125; y = 0.0625, 0.125," 15, no. 11 (2025) 115110.